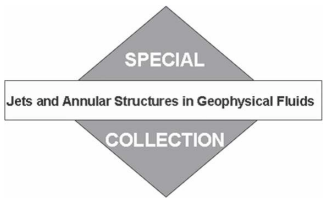

Forced Annular Mode Patterns in a Simple Atmospheric General Circulation Model

MICHAEL J. RING AND R. ALAN PLUMB

Program in Atmospheres, Oceans, and Climate, Massachusetts Institute of Technology, Cambridge, Massachusetts

(Manuscript received 30 April 2006, in final form 26 October 2006)

ABSTRACT

Previous studies using simplified general circulation models have shown that "annular modes" arise as the dominant mode of variability. A simple GCM is used here to explore to what extent these modes are also the preferred response of the system to generic forcing.

A number of trials are conducted under which the model is subjected to an artificial, zonally symmetric angular momentum forcing, and the climatologies of these trials are compared to that of the control. The forcing location is varied among the several trials. It is found that the changes in the model's climatology are generally annular mode–like, as long as the imposed forcing projects strongly upon the annular modes of the unforced model.

The role of changes to the eddy–zonal flow feedback versus the action of direct forcing is also considered through the use of a zonally symmetric version of the model. It is found that the direct responses to forcing are insufficient to capture either the strength or the structure of the annular mode responses. Instead, the changes in eddy fluxes are needed to produce the correct responses.

1. Introduction

The low-frequency patterns known as the annular modes have attracted an increasing amount of research interest in recent years. While the annular modes are the leading patterns of extratropical variability in both hemispheres on a month-to-month time scale (Thompson and Wallace 1998, 2000), their behavior may also be important for deciphering changes over longer periods, such as decadal climate trends (Thompson et al. 2000). The patterns are remarkably robust, and though strongest in winter they are found during the summer as well (Thompson and Wallace 2000). Often defined in terms of pressure or geopotential height, the signature of these patterns may be found in other meteorological fields as well, notably zonal wind (Lorenz and Hartmann 2001, 2003).

A number of studies have shown that annular modes similar to those observed in the earth's atmosphere are produced by models. Even simple two-layer models (e.g., Robinson and Qin 1992; Robinson 1994, 1996) may contain vacillations of the zonal jet like those seen in the atmosphere. Annular modes have also been demonstrated in barotropic models (e.g., Vallis et al. 2004), dynamical cores of general circulation models (e.g., Yu and Hartmann 1993; Polvani and Kushner 2002; Kushner and Polvani 2004), aquaplanet GCMs (e.g., Cash et al. 2002), and full GCMs with more realistic oceans, topography, or chemistry schemes (e.g., Shindell et al. 1999; Kidson and Watterson 1999; Fyfe et al. 1999).

As substantial components of atmospheric variability, these patterns have come to be known as "modes." But is this a meaningful description? If these patterns are truly mode-like, then not only will they appear as unforced natural variability, but also as a preferred response of the atmospheric circulation to external forcings. There are indeed suggestions of such a preferred response in the atmosphere to Antarctic ozone depletion (Thompson and Solomon 2002) and greenhouse forcing (e.g., Shindell et al. 1999; Fyfe et al. 1999; Kushner et al. 2001; Shindell et al. 2001; Rind et al. 2002; Gillett et al. 2002).

We will test that presumption here, using a simple GCM, by subjecting the model atmosphere to a variety of forcings. These forcings are not meant to simulate any real phenomenon in the atmosphere, and their structure does not resemble that of the annular modes. Hence, they should offer a good test as to whether an

Corresponding author address: Michael J. Ring, Program in Atmospheres, Oceans, and Climate, 77 Massachusetts Avenue, Room 54-1715, Cambridge, MA 02139.
E-mail: mring@mit.edu

DOI: 10.1175/JAS4031.1

annular mode–like pattern may arise in response to a generic forcing.

We describe the setup of our model in section 2. A control climatology is produced; we discuss these results in section 3 and describe the annular mode structures that dominate the variability. We then insert artificial forcings, symmetric in longitude but localized in latitude and height, to obtain the forced responses of the model. Several trials with forcings whose magnitudes do not vary with height are also considered. We examine the forced trials in section 4.

In looking at these model results, we will also pay special attention to changes in eddy fluxes that accompany variations in the zonal mean. While the annular modes themselves are zonally symmetric, eddy feedback plays a critical role in maintaining the patterns. Diagnoses of both reanalysis and model results indicate a connection between the annular wind anomalies and eddy activity (Limpasuvan and Hartmann 2000). Lorenz and Hartmann (2001, 2003) found that this relationship between eddies and mean flow represents a positive feedback. Therefore, in sections 3 and 4 we examine the patterns of eddy flux divergence that accompany the annular wind anomalies. Additionally, we conduct trials using a zonally symmetric version of the model to test the role of eddies more explicitly. Results from these runs are shown in section 5. Finally, we offer our discussion and conclusions in section 6.

2. Model setup

We use the dynamical core of the Geophysical Fluid Dynamics Laboratory (GFDL) atmospheric general circulation model in this study. This is a dry, primitive-equation hydrostatic model. The model equations are solved using spectral transforms in the horizontal and Simmons and Burridge (1981) differencing in the vertical. Because no topography is imposed on the surface, our setup is zonally symmetric. In this regard, our runs are similar to those by Kushner and Polvani (2004) in their use of this model.

For the results shown here, the model is run with a T30 spectral resolution, and 20 vertical levels, equally spaced in sigma coordinates from $\sigma = 0.025$ to $\sigma = 0.975$. Rayleigh friction is used to represent surface drag. We choose a coefficient of 2 day^{-1} at the surface, which decreases linearly to zero at $\sigma = 0.7$. Radiation is parameterized by Newtonian cooling to a prescribed, zonally symmetric reference temperature. The cooling rate is 1/40 day^{-1} above $\sigma = 0.7$, but increases linearly to ¼ day^{-1} at the surface. A sixth-order hyperdiffusion, damping the smallest wavelengths present on a time scale of 7/10 day, is also applied. Model results for runs with higher spectral resolutions or damping time scales that varied by a factor of 2 were similar to those shown here.

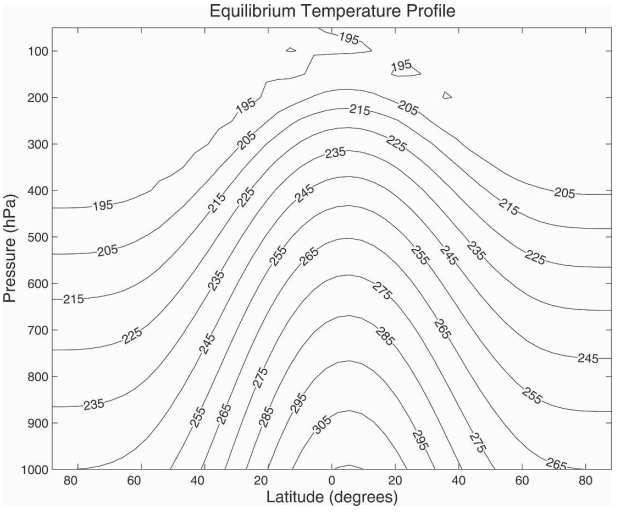

FIG. 1. Equilibrium temperature profile for model runs. Contour interval is 10 K.

Our equilibrium temperature profile is shown in Fig. 1. It is similar to that used by Held and Suarez (1994), but some modifications are made. The point of maximum reference temperature is displaced slightly into the Northern Hemisphere, and an additional term, equal to 10 K multiplied by the sine of latitude, is added to the equilibrium temperature profile. Together, these changes result in a reference temperature profile similar to the temperature profile of austral winter, with the point of maximum equilibrium temperature occurring in the Northern Hemisphere and a larger equator–pole temperature gradient in the Southern Hemisphere than in the Northern Hemisphere. Additionally, the portion of the reference temperature that is symmetric about its maximum value in this profile varies as the fourth power of the cosine of latitude.

Also, we run a zonally symmetric version of the model, which allows us to separate the response contributed directly from the forcing itself from that resulting from changes in eddy fluxes between the forced and control trials. A control climatology is obtained by forcing the zonally symmetric model with the climatological eddy fluxes from the full model run. We then conduct trials, inserting the imposed forcing but not the changes in eddy fluxes from the similar full model run, to discern the change in zonal wind caused by the imposed forcing alone. Finally, runs using the zonally symmetric model, but including both the imposed forcing and changes in eddy fluxes, are conducted and compared to the similar output, including only the directly imposed forcing.

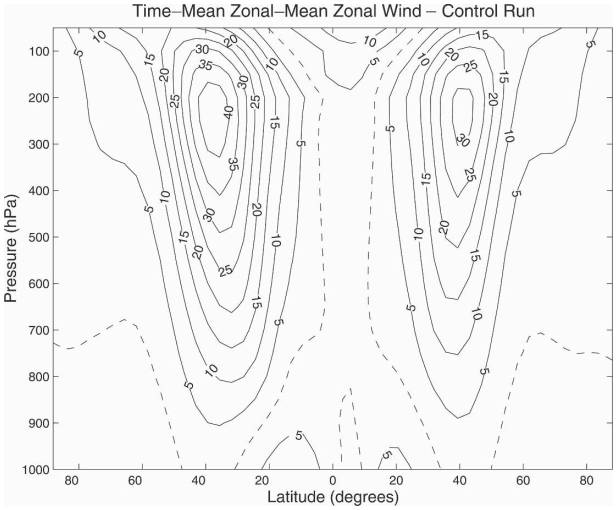

FIG. 2. Zonal- and time-mean zonal wind for the unforced model run. Contour interval is 5 m s^{-1}; zero contour is dashed.

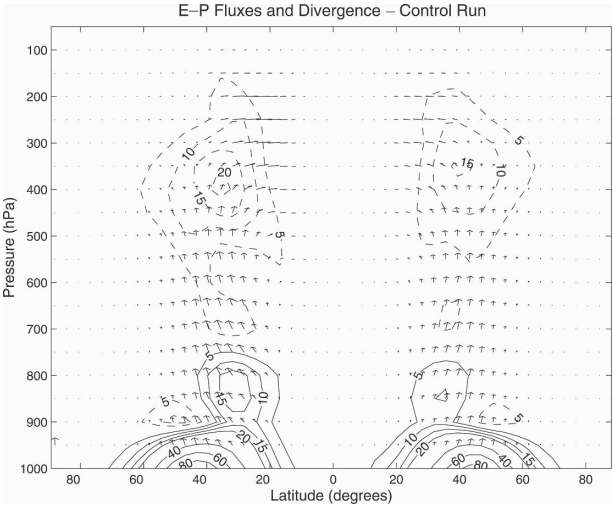

FIG. 3. Time-mean E–P fluxes and divergence from control run plotted according to the scaling in Edmon et al. (1980). Divergence is contoured; interval is 5×10^{15} m^3 until 20×10^{15} m^3 and 20×10^{15} m^3 thereafter. Negative contours are dashed and zero contour is omitted. Arrows represent E-P flux; sample arrow at bottom left represents 5×10^{20} m^3 Pa of upward flux; an equivalent length in the horizontal represents 6.47×10^{15} m^3 of meridional flux.

3. Control climatology

Before examining the results of trials with applied forcing, we first review the climatology of the unforced model run. The results shown here are composed of 7000 days of data, recorded once daily, after the model, starting from rest, had reached a climatologically steady state. The climatologies and patterns of variance shown below are robust and obtainable from smaller segments of the model climatology. The results shown here have been interpolated onto pressure surfaces from sigma surfaces.

The time-mean, zonal-mean zonal wind is illustrated in Fig. 2. The profile of zonal wind is similar to that found in the atmosphere, although some differences do exist. The strongest wind is found at the center of the Southern Hemisphere (winter) jet, located at about 37°S and 250 hPa. The wind speed peaks at 43 m s^{-1} in the jet core and drops to slightly more than 2 m s^{-1} at the surface maximum. The Northern Hemisphere (summer) jet is located near 41°N, placing it slightly poleward relative to its austral counterpart. In our discussions of the forced model runs in section 4, we will compare the zonal wind fields obtained in those trials to these results.

The climatological Eliassen–Palm (E–P) flux and divergence are shown in Fig. 3. The dominant pattern is an upward flux associated with the generation and dissipation of baroclinic eddies, with divergence at lower altitudes and convergence at higher altitudes. Near the level of the jets, there is some equatorward propagation of E–P flux as well. Most of the divergence is baroclinic (i.e., stemming from the vertical divergence), but the barotropic (meridional) divergence is important as well, particularly in the upper troposphere. This behavior is consistent with that found by Edmon et al. (1980).

The annular mode is the strongest pattern of variability in the model, and its signature is visible in several fields. Here we show the patterns in the surface pressure field in Fig. 4. The time-mean values have been removed, and the leading EOF of the anomalies in each hemisphere is computed. Both hemispheres show the dipolar exchange of mass between midlatitude and polar regions (Thompson and Wallace 1998, 2000). Notably, the patterns are highly zonally symmetric, with belts of anomalous pressure encircling the entire globe in both hemispheres. Given the strong longitudinal symmetry evident in these patterns, we will focus on the behavior of the zonal means in the remainder of this paper.

Figure 5 displays the leading EOFs of the zonal-mean zonal wind anomalies. Unlike the pressure EOFs shown above (which were calculated separately in each hemisphere), the wind EOFs are computed on the global domain; however, with no spatial overlap between the two leading patterns we have displayed them on the same plot. EOF1 is confined to the Southern Hemisphere and EOF2 to the Northern Hemisphere, and the global patterns are similar to those obtained when examining each hemisphere separately. The patterns show the characteristic north–south shift of the jet ob-

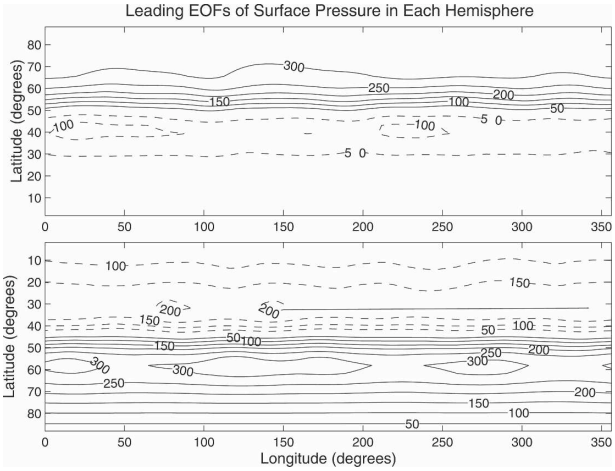

FIG. 4. (top) First EOF of surface pressure anomalies in the Northern Hemisphere. The time-mean values are removed before computing the EOF. Contour interval is 50 Pa; negative contours are dashed. (bottom) As in the top panel, but for the Southern Hemisphere.

served in the atmosphere as the signature of the annular mode in that field (Lorenz and Hartmann 2001, 2003).

The leading EOFs of the E–P flux divergence (not shown), which suggest increased or decreased eddy generation and upward propagation, are not particularly elucidating for understanding the zonal wind variability. Instead, we conduct a singular value decomposition (SVD) of the covariance matrix between the zonal wind anomalies and E–P flux divergence anomalies to examine the connection between the variability

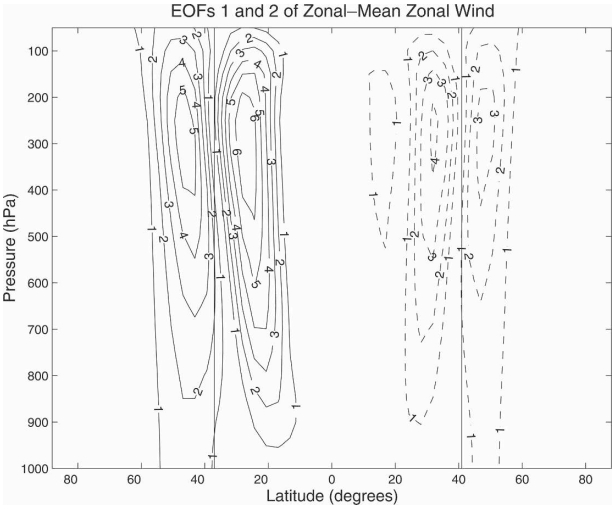

FIG. 5. First and second EOFs of zonal-mean zonal wind anomalies. Solid lines are contours of the leading EOF; dashed lines are contours of the second EOF. Contours are in units of 1 m s^{-1}; vertical lines indicate positions of time-mean jets.

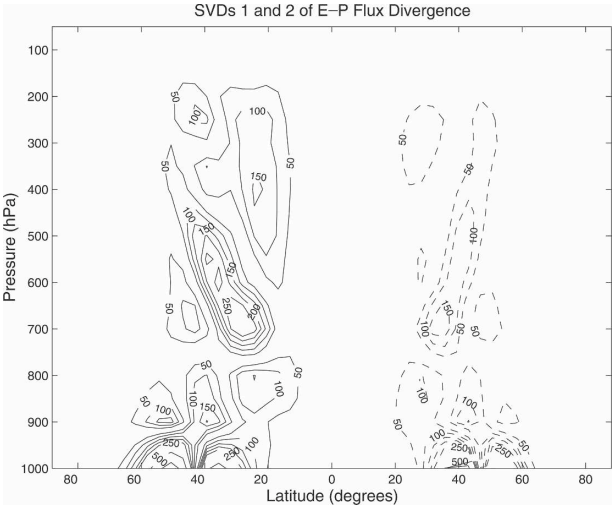

FIG. 6. Leading spatial patterns of E-P flux divergence anomalies derived from SVD analysis with the zonal wind anomalies. Solid lines indicate the leading pattern; dashed lines indicate the second pattern. Contour interval is 50 m^2 s^{-2} until 250 m^2 s^{-2} and 250 m^2 s^{-2} thereafter.

of the two quantities. While the leading spatial pattern of the wind that emerges from the operation is virtually identical to that of the EOF of the wind, the leading spatial pattern of the E–P flux divergence is quite different from that of its "natural" EOF. The first and second leading patterns of the divergence found through this analysis are shown in Fig. 6.

These leading spatial patterns are noteworthy for several reasons. First, the lower-level E–P flux divergence migrates with the zonal wind. In the positive phase of the annular mode (associated with a jet poleward of its time-mean position), increased eddy generation is observed poleward of the location of the time-mean maximum. The converse is true in the negative phase. In the upper troposphere, E–P flux divergence anomalies also migrate with the position of the jet; positively anomalous divergence is found in the upper troposphere where the surface anomalies are also positive, and negative upper-tropospheric anomalies occur at the same latitude as the negative surface anomalies.

In summary, the control climatology of our model produces annular modes similar to those observed in the real atmosphere. These patterns are associated with anomalies in the E–P flux divergence, which act to sustain the annular mode patterns. With these results in mind, we now turn to the response of the model under the influence of artificial torques.

4. Forced climatologies

Having examined the climatology of the control run, we now review the responses of the model to the addi-

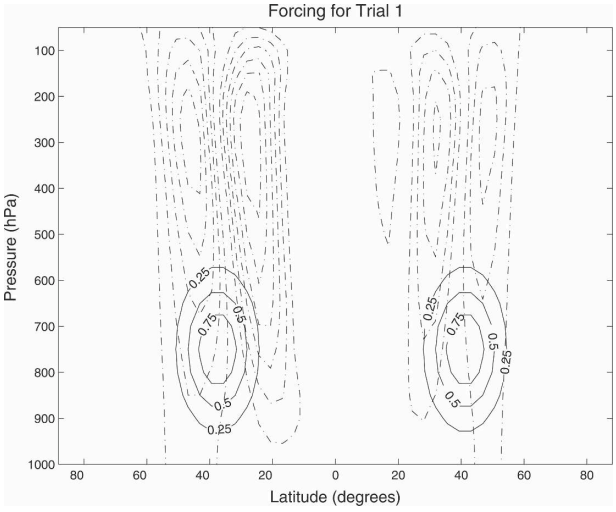

FIG. 7. Torque applied in trial 1. Forcing contours are in m s^{-1} day^{-1} acceleration of angular momentum. Dotted lines are leading EOFs of zonal-mean zonal wind.

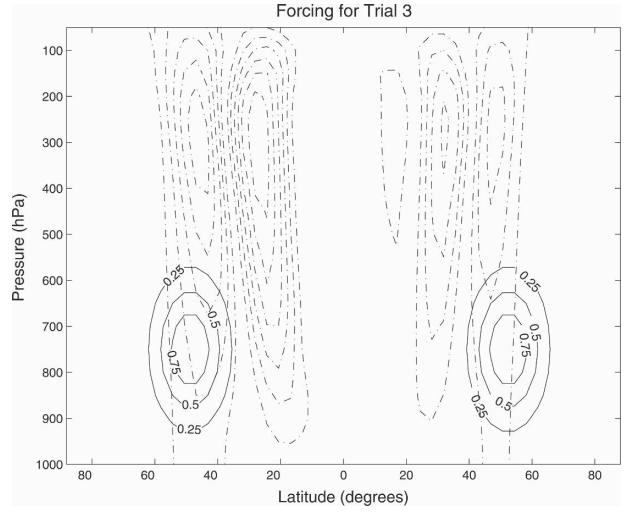

FIG. 8. As in Fig. 7, but for trial 3.

tions of angular momentum forcings. Below we will discuss the results of a suite of experiments, with the torques centered in different locations. Most trials use vertically localized forcings, but we conduct several trials using barotropic forcings as well.

In each case we implant the angular momentum forcings into a selected day of the control run, turn them on smoothly over a period of 20 days, and then hold their magnitudes steady for the duration of the run. Lengthening the switch-on time for selected trials did not result in climatologies different than those shown here.

Figures 7 and 8 show the forcings used in two of our trials (numbered 1 and 3, respectively, in Table 1). These torques are similar to those used by Song and Robinson (2004). The forcing is dipolar globally, but monopolar in each hemisphere; no net angular momentum is added or subtracted globally. These forcings are zonally symmetric but Gaussian in latitude and pressure. The *e*-folding decay scales of the forcing strength are about 11° in the horizontal and 150 hPa in the vertical. Note that while the forcings in Fig. 7 are centered at the nodes of the EOF of zonal wind in each hemisphere, the forcings in Fig. 8 project strongly onto the EOFs.

Table 1 summarizes the changes in the positions of the vertically localized forcings used in the various trials. In the first six trials, we investigate the response of the model to forcings located at the jet center, on the jet's poleward flank, and on the jet's equatorward flank, respectively, for forcings placed in both the lower and upper troposphere. Trial 7 features a forcing centered in between those used in trials 1 and 3. A forcing located poleward of that in trial 3 is employed in trial 8. For each trial, the amount of angular momentum added to each hemisphere is the same as that in the other runs.

All but one of the runs shown below use climatologies of 5000 days, which are sampled once daily. This length of time was found to yield statistically robust results in most of the runs. Only trial 6 uses a 7000-day climatology.

The change in zonal wind from the control run of the model for each of the eight trials is shown in Fig. 9. In trials 1 and 2, which feature a weak projection of the forcing onto the annular modes, the forced responses match poorly with the annular modes. In trial 1, the response in each hemisphere is weak and monopolar. The response in trial 2 is dipolar in the upper troposphere of the Southern Hemisphere, but the dipole does not extend to the ground as in the other trials. The response to that trial in the Northern Hemisphere is monopolar.

The other six trials (trials 3 through 8), in which the

TABLE 1. Summary of trials with imposed vertically localized angular momentum forcings.

Trial No.	Latitude of forcing center	Level of forcing center
1	Jet center	750 hPa
2	Jet center	250 hPa
3	11° poleward of jet center	750 hPa
4	11° poleward of jet center	250 hPa
5	11° equatorward of jet center	750 hPa
6	11° equatorward of jet center	250 hPa
7	5.5° poleward of jet center	750 hPa
8	16.5° poleward of jet center	750 hPa

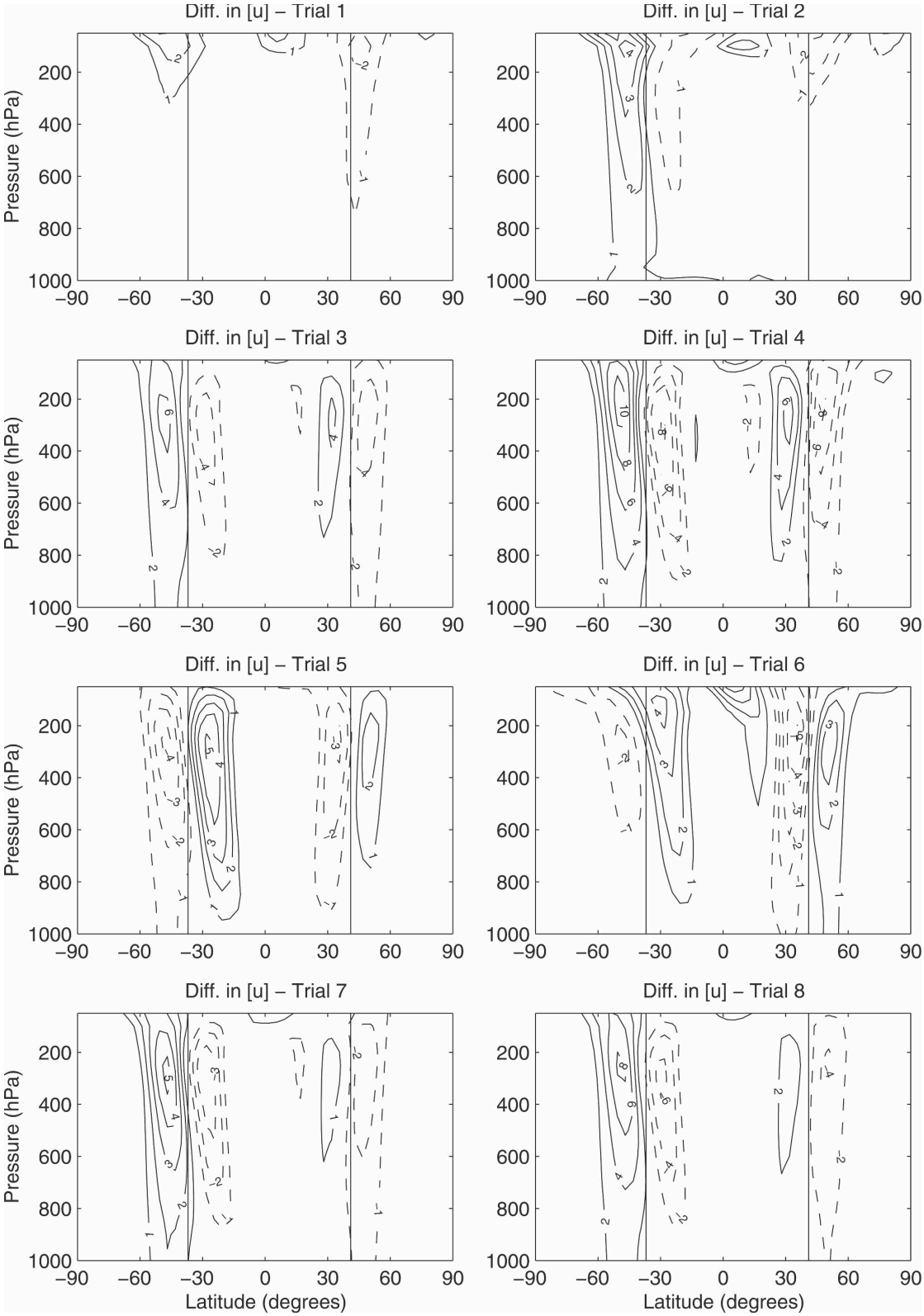

FIG. 9. Difference in time-mean zonal-mean zonal wind for each trial vs the control. Contour interval is 1 m s^{-1} for trials 1, 2, 5, 6, and 7 and 2 m s^{-1} otherwise. Solid vertical lines are positions of time-mean jets.

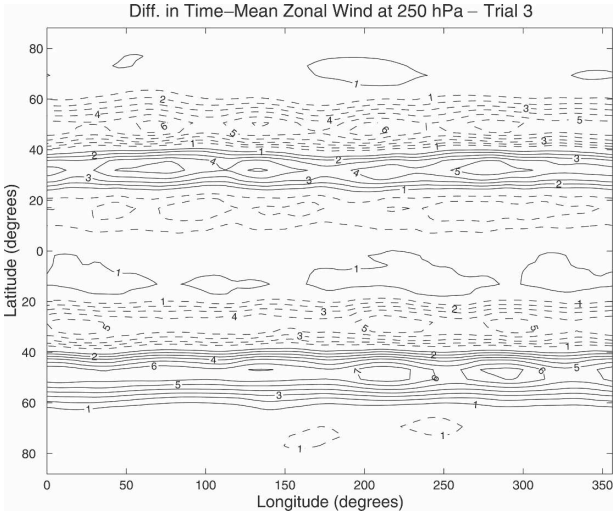

FIG. 10. Difference in 250-hPa zonal wind between trial 3 and the control run. Contour interval is 1 m s^{-1}.

imposed torques project strongly onto the annular modes of the control run, feature annular mode–like patterns as the model response. Each of these cases features a zero anomalous wind contour at or very close to the center of the unforced jet, while regions of anomalously positive or negative zonal wind are found on each side of the node. The responses are found in both hemispheres, and the regions of anomalous wind extend throughout the depth of the model.

In Fig. 10, we examine the longitudinal structure of these changes for an example case. Not surprisingly, the difference in the time-mean zonal wind at 250 hPa for trial 3 versus the control is highly zonal, similar to the pattern of pressure EOFs shown earlier from the control run (Fig. 4). The belts of strengthened or weakened westerlies reach across all longitudes. Choosing a different trial or different pressure level yields similar results.

Because the zonal wind anomalies are closely intertwined with those of the E–P flux divergence, we next examine the difference between the E–P flux divergence in the forced trials versus the unforced model run (Fig. 11). Mirroring the differences in zonal wind, the changes in the E–P flux divergence from the control run resemble the SVD pattern shown in Fig. 6 in those cases for which an annular mode–like response is present.

In trials 3 through 8, the changes in E–P flux divergence are similar to the patterns from the unforced model run. The changes in E–P flux divergence at the ground are dipolar, indicating the migration of eddy generation with the jet suggested in the SVD analysis. Patterns in the middle and upper troposphere also resemble the SVD pattern. (For ease of comparison with the SVD pattern in Fig. 6, the same contour interval is chosen. At a reduced contour interval, the similarities in the structure of the responses in the upper troposphere are more evident.) In contrast, the changes in E–P flux divergence from trials 1 and 2 do not resemble the SVD pattern.

From these eight trials, we note that the zonal wind response of the system to the applied torques is dipolar and annular mode–like, as long as the applied forcing projects well onto the annular mode patterns of the unforced run. From Figs. 9 and 11, it is also clear that a forced change in zonal wind resembling the annular mode patterns of the unforced model is accompanied by a change in E–P flux divergence that resembles the unforced run's SVD pattern. These results strongly suggest that the eddy feedback plays a critical role in determining the wind response. We will consider this point further in the next section through the use of a zonally symmetric model.

As a further test, we consider four trials that involve torques whose strength does not vary with pressure. We run four such "barotropic" cases, composed of trials with forcing inserted on the poleward and equatorward flank. As in the previous cases, the variation of forcing strength with latitude is Gaussian. For each location, two runs are conducted—one uses a positive torque in the Southern Hemisphere and a negative torque in the Northern Hemisphere, and the other uses the reverse polarity. For these trials, the vertically integrated forcing applied here is the same as that from the trials using vertically localized forcing. Hence, the magnitude of maximum forcing is decreased by approximately a factor of 4. These trials are summarized in Table 2. The lengths of climatologies derived for these trials are 5000 days for trials 9 and 10, and 7000 days for trials 11 and 12.

Trials 9 and 10, which feature forcings applied on the poleward flanks of the jets, result in robust annular mode patterns, as shown in Fig. 12. Note that the patterns occur in both hemispheres for both positive and negative polarities of the forcing. Trial 11 also produces a dipolar response in both hemispheres, though the magnitude of the wind patterns is reduced from the responses in trials 9 and 10. The anomalies here are similar to those found in trial 6, which used a forcing placed at the same latitude but vertically localized in the upper troposphere. The response to trial 12 includes a strong annular mode pattern in the Southern Hemisphere, but no such pattern in the Northern Hemisphere. The changes in E–P flux divergence found in trials 9 through 12 follow from what is expected by the zonal wind changes. In trials 9 and 10 the changes are strong and mimic the SVD pattern shown earlier. In

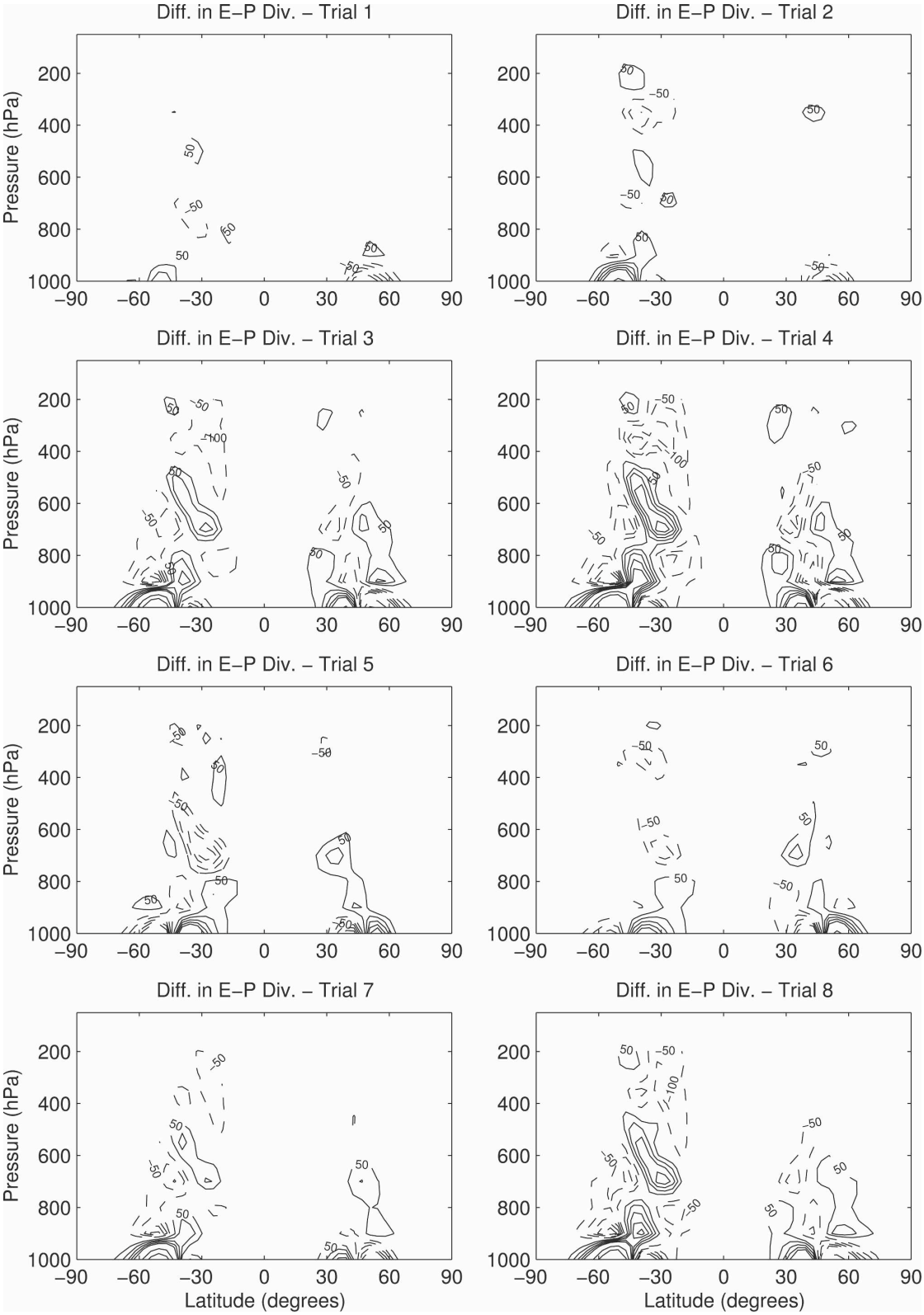

FIG. 11. As in Fig. 9, but for E–P flux divergence. Contour interval is 50 $m^2 s^{-2}$ until a magnitude of 250 m s^{-2} and 250 $m^2 s^{-2}$ thereafter.

TABLE 2. Summary of trials with imposed barotropic angular momentum forcings.

Trial No.	Latitude of forcing center	Polarity of Southern Hemisphere forcing
9	11° poleward of jet center	Positive
10	11° poleward of jet center	Negative
11	11° equatorward of jet center	Positive
12	11° equatorward of jet center	Negative

trials 11 and 12, however, the changes are weaker (Fig. 13).

Finally, we summarize the results of the 12 trials by comparing the projections of the wind responses onto the unforced EOF with the projections of the forcing onto the EOF. The Southern Hemisphere responses and forcing are projected onto the Southern Hemisphere EOF, and the same procedure is used independently for the Northern Hemisphere. The results, shown in Fig. 14, indicate that the pattern between the strengths of the two projections is linear, showing that generally the strength of the annular mode response to the forcing should scale as the strength of the projection of the forcing in these types of trials.

In summary, the response of the model to the applied torques is annular mode–like in most cases for which the forcing projects upon the annular mode, although the response is weak for some cases with forcing placed on the equatorward side of the jet. When an annular mode pattern is found, the changes in E–P flux divergence strongly resemble the structure found from SVD analysis in the unforced run, suggesting the eddies are determining the response. We examine this more explicitly using the zonally symmetric model.

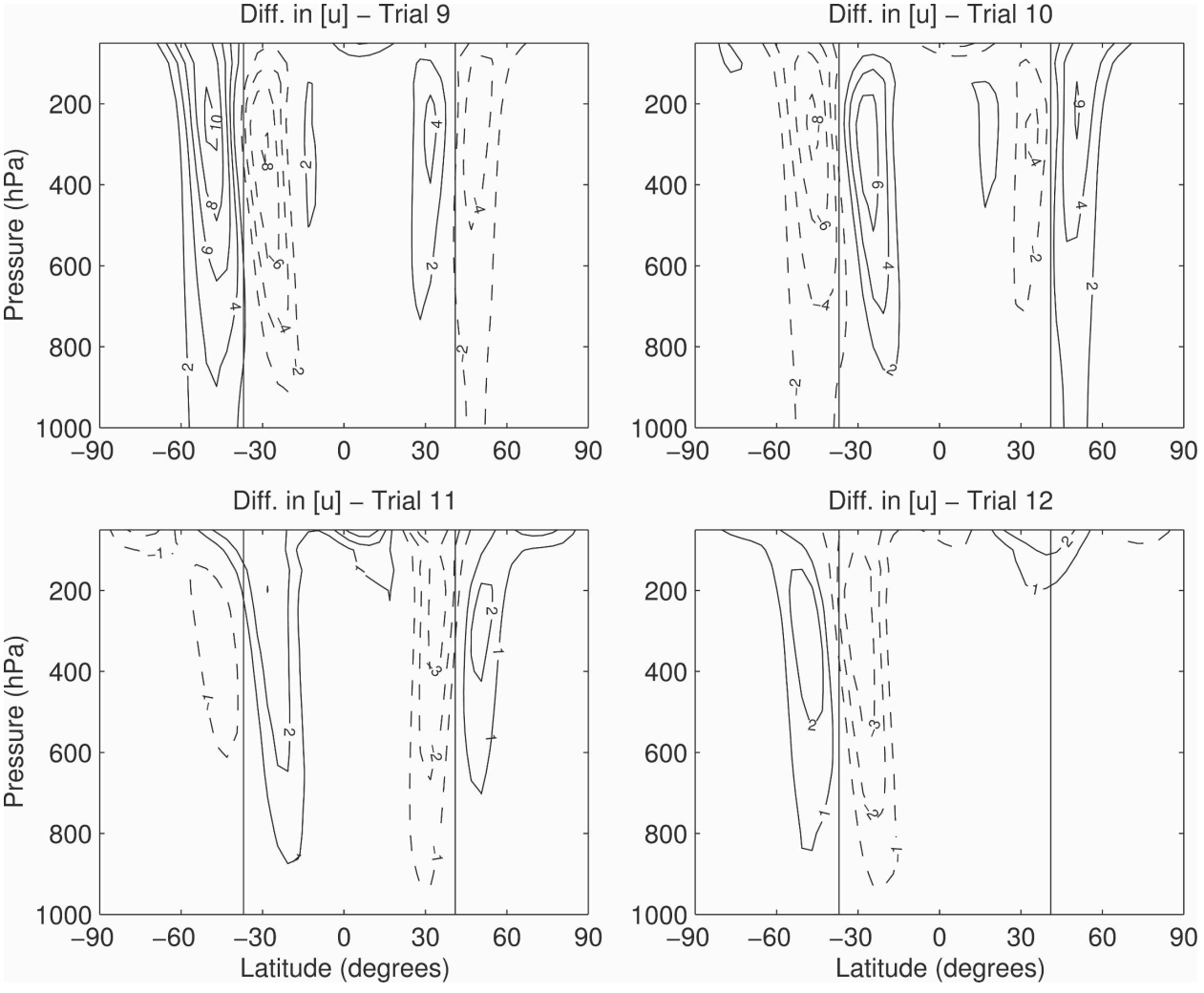

FIG. 12. Difference in time-mean zonal-mean zonal wind for each trial with barotropic forcing vs the control. Contour interval is 2 m s^{-1} for trials 9 and 10 and 1 m s^{-1} for trials 11 and 12.

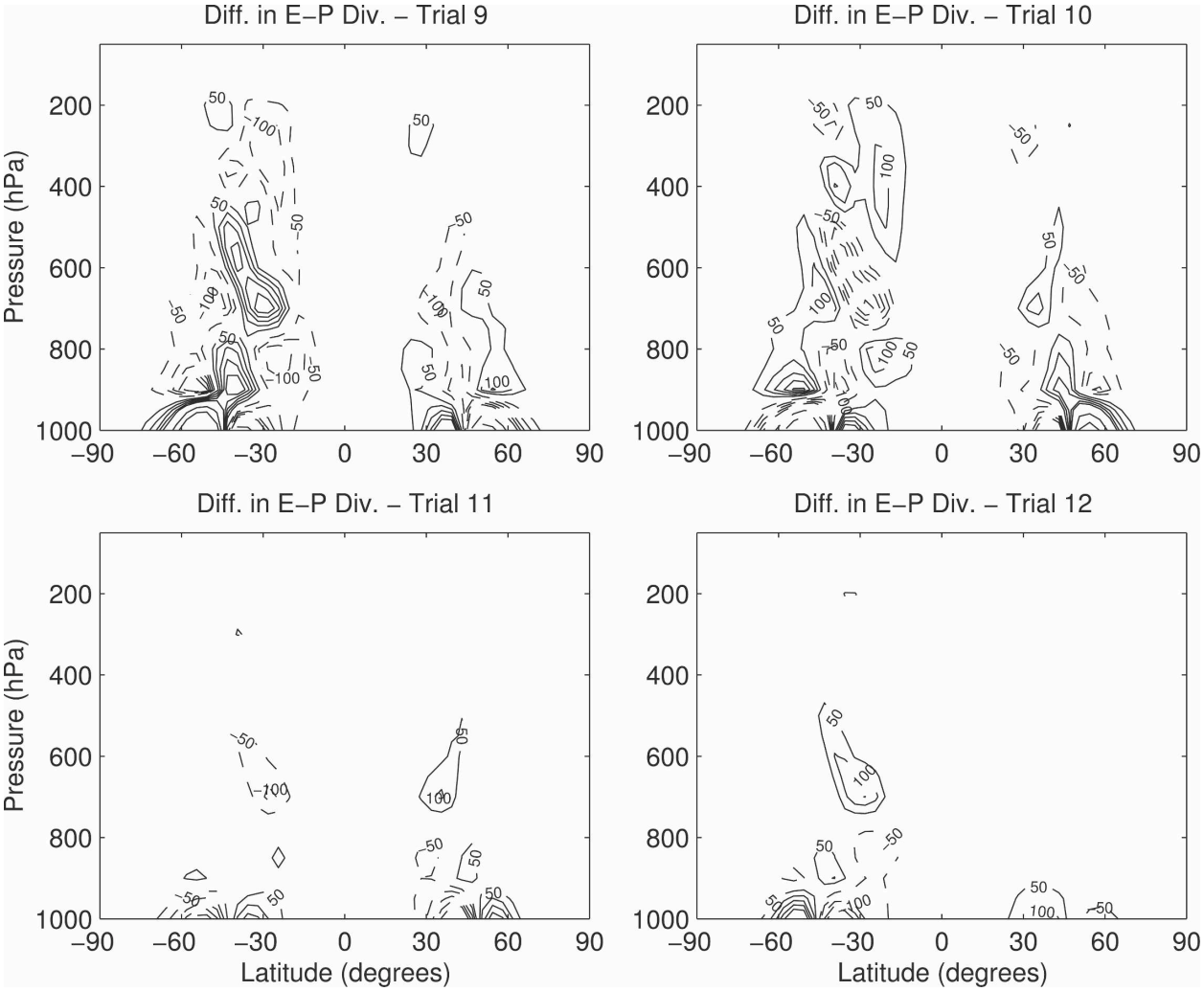

FIG. 13. As in Fig. 12, but for E–P flux divergence. Contour interval is as in Fig. 11.

5. Diagnoses using a zonally symmetric model

To learn more about the model responses to the applied forcings, we use a zonally symmetric version of the model in which the eddy fluxes must be prescribed. The zonally symmetric model is first run using the climatological eddy fluxes calculated from the control run, which provides a good reproduction of the full model's climate. Next, for each trial two forced cases are conducted. In one case, the zonally symmetric model is run including the applied torque, *but keeping the same climatological eddy fluxes derived from the control run*, to examine the direct effects of the applied torque without eddy feedback. Finally, the zonally symmetric model is run including both the applied torque and the climatological eddy fluxes derived from the perturbed full model run. The results shown below are averaged over the final 500 days of 2000-day model runs.

In each case in which an annular mode response was found, it is clear from runs using the zonally symmetric model that the zonal wind responses found in the full model cannot be derived from direct forcing alone. As should be expected, the direct responses to the monopolar forcings are predominantly monopolar, with the strongest response at the latitude of the forcing. The addition of eddy flux changes is necessary to capture both the correct strength and shape of the wind responses in the zonally symmetric model.

First we examine the responses to forcing on the poleward flanks of the jets, using trials 3 and 4 as our examples. These are shown in Fig. 15; the full model results from these trials are on the second row of Fig. 9. In both cases the wind response to the direct forcing only is substantially monopolar, as seen in the top two panels of the figure. In the upper troposphere there are centers of opposite-signed wind anomalies, but the

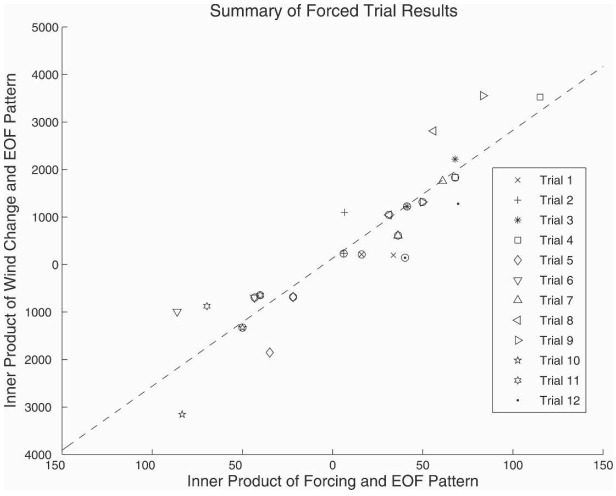

FIG. 14. Inner product of zonal wind change and EOF pattern plotted against inner product of forcing and EOF pattern. Plot contains points for both Southern Hemisphere and Northern Hemisphere; NH points are enclosed with a circle and rotated to appear in same quadrant as similar SH trial. Dashed line is best least squares linear fit.

strongest wind response occurs at the latitude of the forcing, with the same sign as the forcing. Noteworthy as well are the magnitudes of the direct responses—they are weaker in the lower and middle troposphere than those derived from the full model run (this is true throughout the atmosphere for the run using forcing from trial 3). Clearly, the direct responses alone can explain neither the magnitudes of the full model responses nor their annular mode–like structures.

The bottom two panels of Fig. 15 display results from the zonally symmetric model for the addition of both the applied torques and the eddy flux changes from the full model. Here the annular mode patterns are reproduced. The addition of the eddy flux changes allows for both the correct shape and magnitude of the responses to be captured in each hemisphere. Hence, the role of the direct forcing is not to produce the annular mode patterns themselves, but rather to activate the eddy–mean flow feedback that produces the annular modes.

We also consider zonally symmetric runs using forcing placed on the equatorward flank. Recall from Fig. 9 that the placement of the torques in these trials resulted in annular mode–like responses in both hemispheres, though the Southern Hemisphere response was noticeably weaker in trial 6. As shown in Fig. 16, the direct responses to the added forcings are again unable to reproduce the changes found in the full model runs, particularly for trial 5. The changes in zonal wind, as expected for inclusion of direct forcing alone, are centered about the latitude of the forcing. Opposite-signed anomalies are present in both trials poleward of the main responses, but these secondary features are weaker than the respective primary anomalies. Including the eddy changes as well as direct forcing produces better results, as shown in the bottom panels of Fig. 16. The zonally symmetric results offer a good match to the full model results for trial 5. The changes found in the zonally symmetric model for trial 6 are less faithful to the details of the full model run. However, the zonally symmetric model does correctly produce the gross pattern.

Turning back to the direct responses shown in Figs. 15 and 16, we note that the latter trials (which use the equatorial-flank forcing) feature a stronger direct response as compared to their poleward-flank counterparts. This is not surprising; consider, for example, the following transformed Eulerian-mean momentum balance:

$$\frac{\partial u}{\partial t} + v^*\left(\frac{\frac{\partial (u\cos\phi)}{\partial \phi}}{a\cos\phi} - f\right) + \omega^*\frac{\partial u}{\partial p} = -c_d u + \frac{1}{a\cos\phi}\nabla\cdot\mathbf{F} + G.$$

For a steady-state response to an external forcing G away from the frictional boundary layer, which includes no changes to the E–P flux divergence $\nabla\cdot\mathbf{F}$, G must be balanced by changes in the meridional circulation (primarily v^*). But, because the magnitude of the absolute vorticity decreases as one draws closer to the equator, the direct response of the meridional velocity must be larger for a forcing placed closer to the equator than for the same strength of forcing placed closer to the pole. Also, the torques placed closer to the equator overlap with the Hadley cell, introducing factors into the dynamics other than the extratropical eddy–mean flow interaction that is crucial to the annular modes.

Consideration of changes to the other dynamic variables also shows the stronger direct response to the forcing for trials with equatorward-flank forcing. For example, consider the changes to streamfunction shown in Figs. 17 and 18. With forcing placed on the poleward flank (Fig. 17), the direct changes in streamfunction are weaker than with the forcing on the equatorward flank (Fig. 18). Additionally, in the former cases the direct changes are clearly extratropical, while in the latter cases the largest direct changes occur at tropical and subtropical latitudes. In trial 5 these changes are primarily confined to the lower troposphere, but in trial 6 large direct changes extend to the tropopause, suggesting substantial interference with the Hadley circulation. Indeed, the streamfunction responses from the zonally symmetric model, including the eddy flux changes, re-

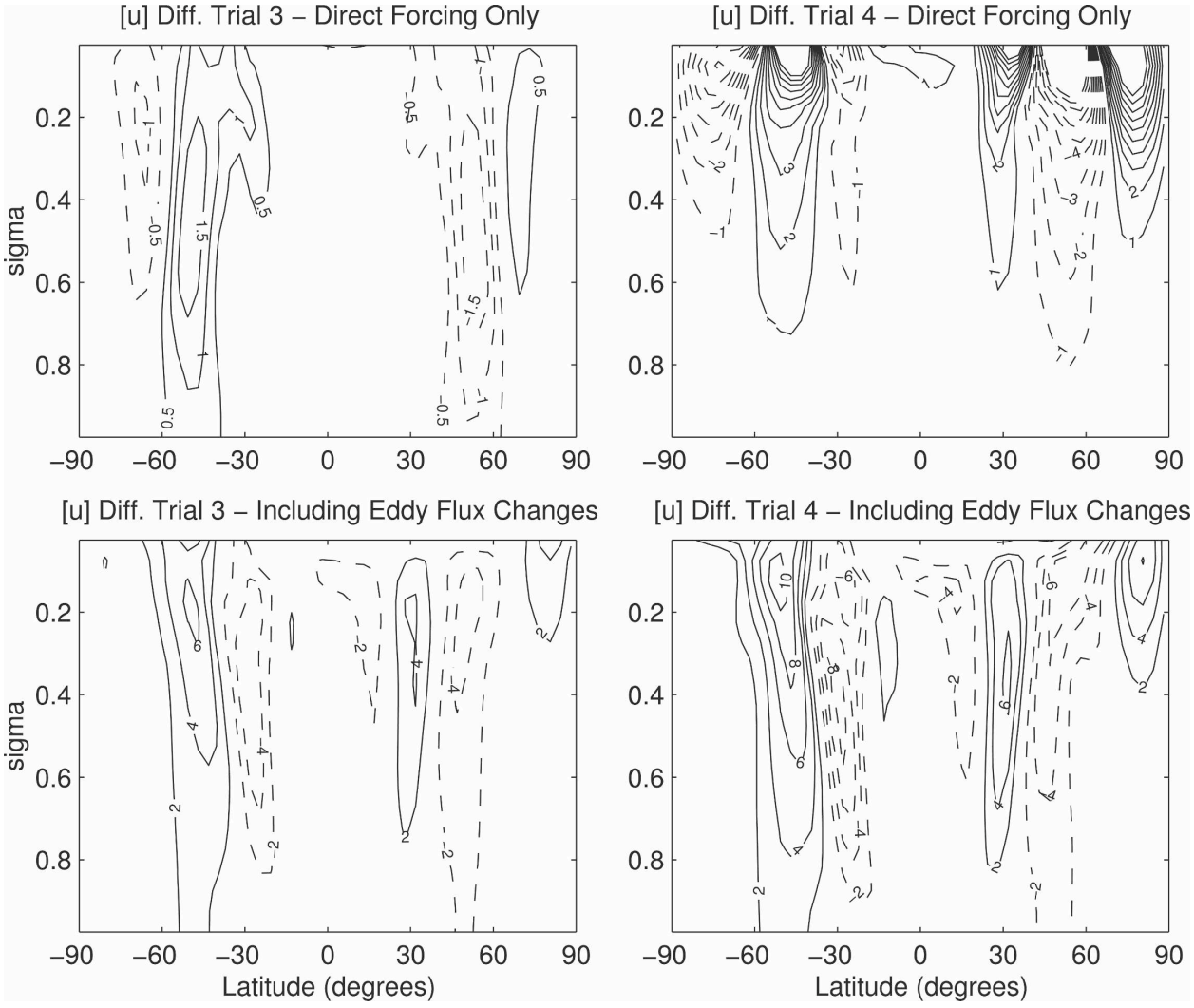

FIG. 15. Response of zonally symmetric model for the indicated trials. (top left) Difference in zonal-mean zonal wind for addition of forcing from trial 3, but no changes to eddy fluxes. (top right) As in top left, but for forcing from trial 4. (bottom left) As in top left, but for addition of both the applied forcing and the changes in eddy fluxes derived from the full model in trial 3. (bottom right) As in bottom left, but for trial 4. Contour interval is 0.5 m s^{-1} in top left panel, 1 m s^{-1} in top right panel, and 2 m s^{-1} in the other panels.

tain much more of the structure of the direct forcing response for the equatorward-flank cases, particularly for trial 6. For this trial, the changes in streamfunction in the midlatitude regions where the annular modes occur are much weaker than those found in trials 3 and 4, and indeed also for trial 5 as well when comparing the Southern Hemisphere responses.

This also offers an explanation for the curious result that the zonal wind response decreased between trials 5 and 6 for the Southern Hemisphere, but increased for the Northern Hemisphere. The Southern Hemisphere is the winter hemisphere in this model, and therefore features stronger Hadley cell dynamics. Also, the position of the forcing is the same in each hemisphere relative to the unforced jet center, but because the Southern Hemisphere jet is located slightly equatorward of its counterpart, so too does the Southern Hemisphere forcing reach a bit more into the Tropics. Hence, the direct response to trial 6 in the Southern Hemisphere is larger than its Northern Hemisphere counterpart (note particularly the direct streamfunction responses in Fig. 18). The annular mode dynamics may be more obscured in the Southern Hemisphere, and the annular mode response is therefore weaker.

6. Summary and discussion

A simple general circulation model is subjected to applied angular momentum forcings to learn whether the annular mode patterns arise in response to the

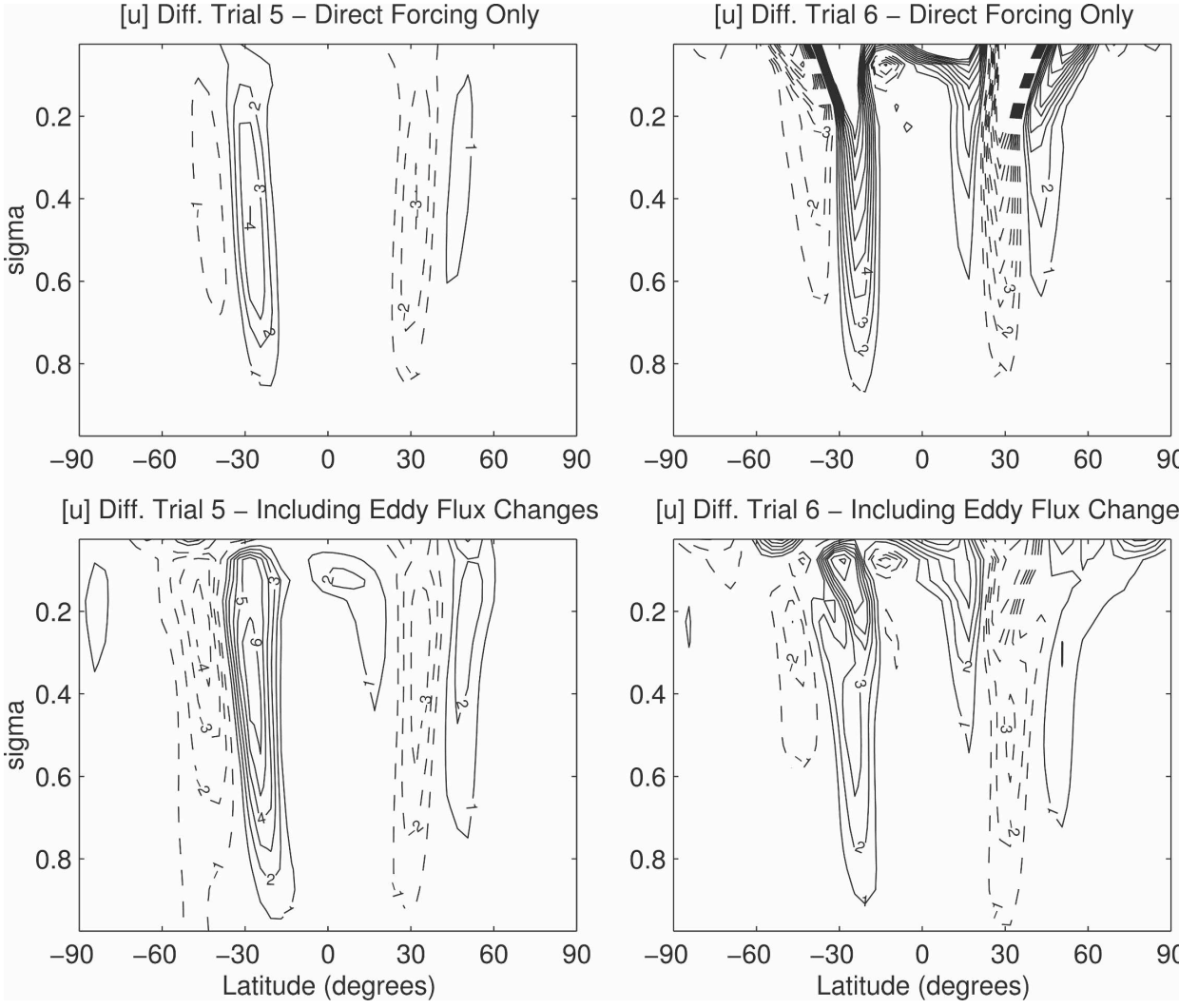

FIG. 16. As in Fig. 15, but for trials 5 and 6. Contour interval is 1 m s^{-1} in all panels.

given forcings. The patterns are found for a number of forcings, suggesting that their given name of "mode" is not without justification. The trials considered here illustrate a linear response between the projection of the applied forcing versus the projection of the forced zonal wind response on the unforced run's annular modes.

Through use of the zonally symmetric model, we determine that the direct forcing alone is not able to produce the correct strength and structure of the annular mode patterns. Instead, the eddy feedback is necessary to produce the correct shape and amplify the magnitudes of the responses, particularly in the lower and middle troposphere.

The dipolar response is strong for most forcings that project strongly onto the annular mode pattern of the unforced run. Two trials with torques centered on the nodal line of the mode did not produce an annular mode–like response. But, a robust annular mode–like response was found for all trials with forcing placed on the poleward flank of the unforced jets' time-mean positions.

The situation is more complicated for trials using forcings placed on the jets' equatorward flanks. While annular mode patterns may be found, in several cases they are not as robust as those from similar trials using forcing on the poleward flank. In particular, while placing forcing in the lower troposphere produces a strong annular mode–like pattern, using forcing placed in the upper troposphere or barotropic forcing does not yield as prominent of a dipole.

The differences between trials using forcing placed on the equatorward flank versus those forced on the poleward flank may be traced to the stronger direct responses in the former trials. For the latter trials, the

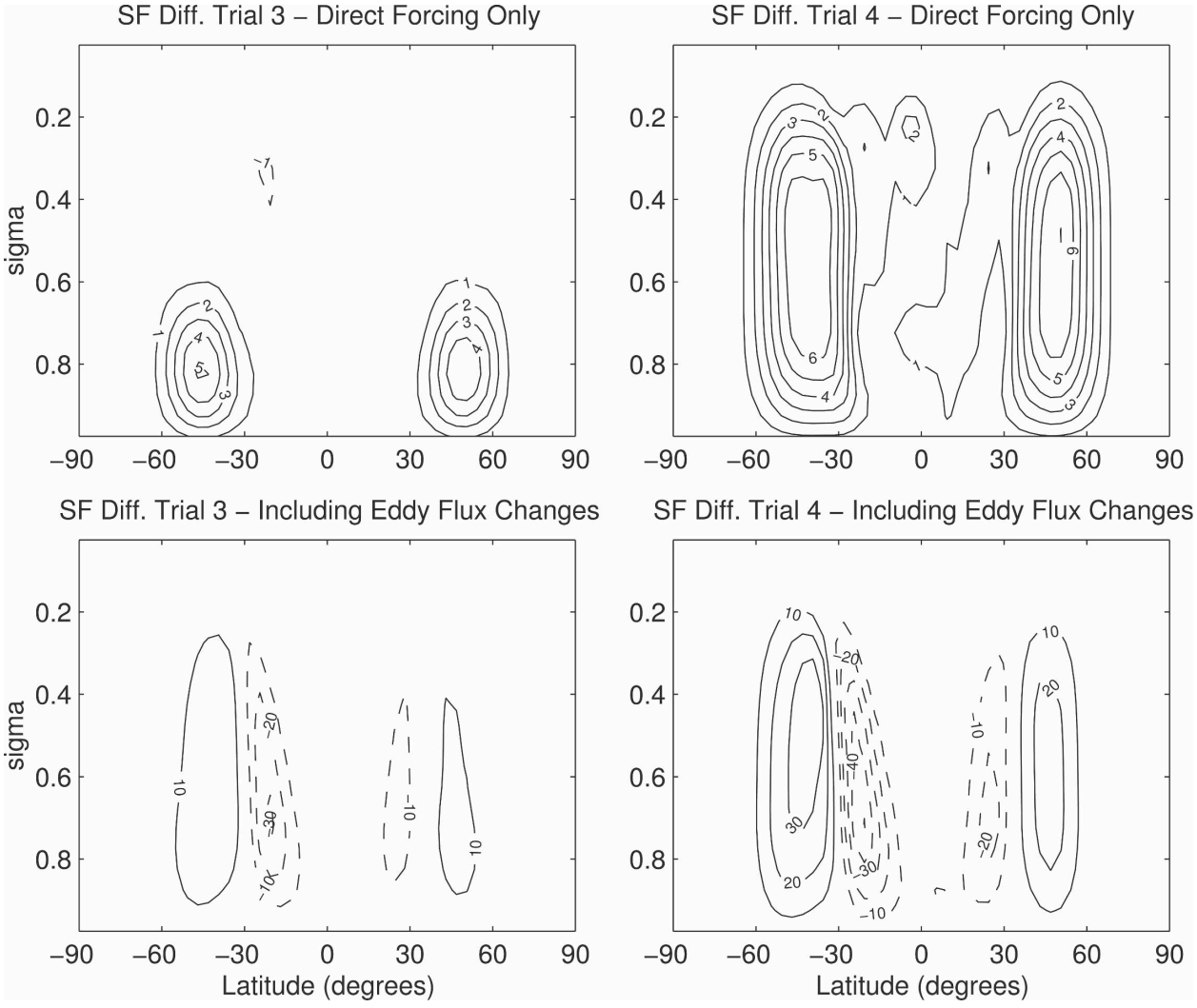

FIG. 17. As in Fig. 15, but for the streamfunction. Contour interval is 1×10^9 kg s^{-1} in top two panels and 10×10^9 kg s^{-1} in bottom two panels.

changes in the meridional circulation calculated from the direct forcing are weak and primarily in the midlatitudes. In contrast, the forcings placed on the equatorward flank offer stronger direct responses, which interfere with the dynamics of the Hadley cell. Therefore, the response may not be solely determined by the changes in eddy fluxes, but retains a larger flavor of the direct response. Still, the eddy feedback must be present because dipolar patterns are generally observed in these trials as well.

In these trials, we have used zonally symmetric forcings of two different shapes (Gaussian bull's-eyes and barotropic forcings). A natural extension of the trials presented here is to employ torques of different shapes in forcing the model. Given our finding that the annular mode response in these trials is proportional to the projection of the imposed forcing, we should expect that they arise in response to other torques than just the ones shown here, depending on the strength of the projection.

The trials discussed here only consider forcings placed in the troposphere. However, the annular modes are also observed in the winter stratosphere, and the patterns may be important in the coupling between the stratosphere and troposphere, and the suspected downward influence of the former on the latter (Baldwin and Dunkerton 1999; Thompson and Wallace 2000; Baldwin and Dunkerton 2001). While the stratosphere is not considered here, the tendency of forcings to amplify the eddy–mean flow feedback may be important in explaining annular mode–like responses because they relate to the stratosphere as well. Model studies have shown that stratospheric perturbations may have an enhanced tro-

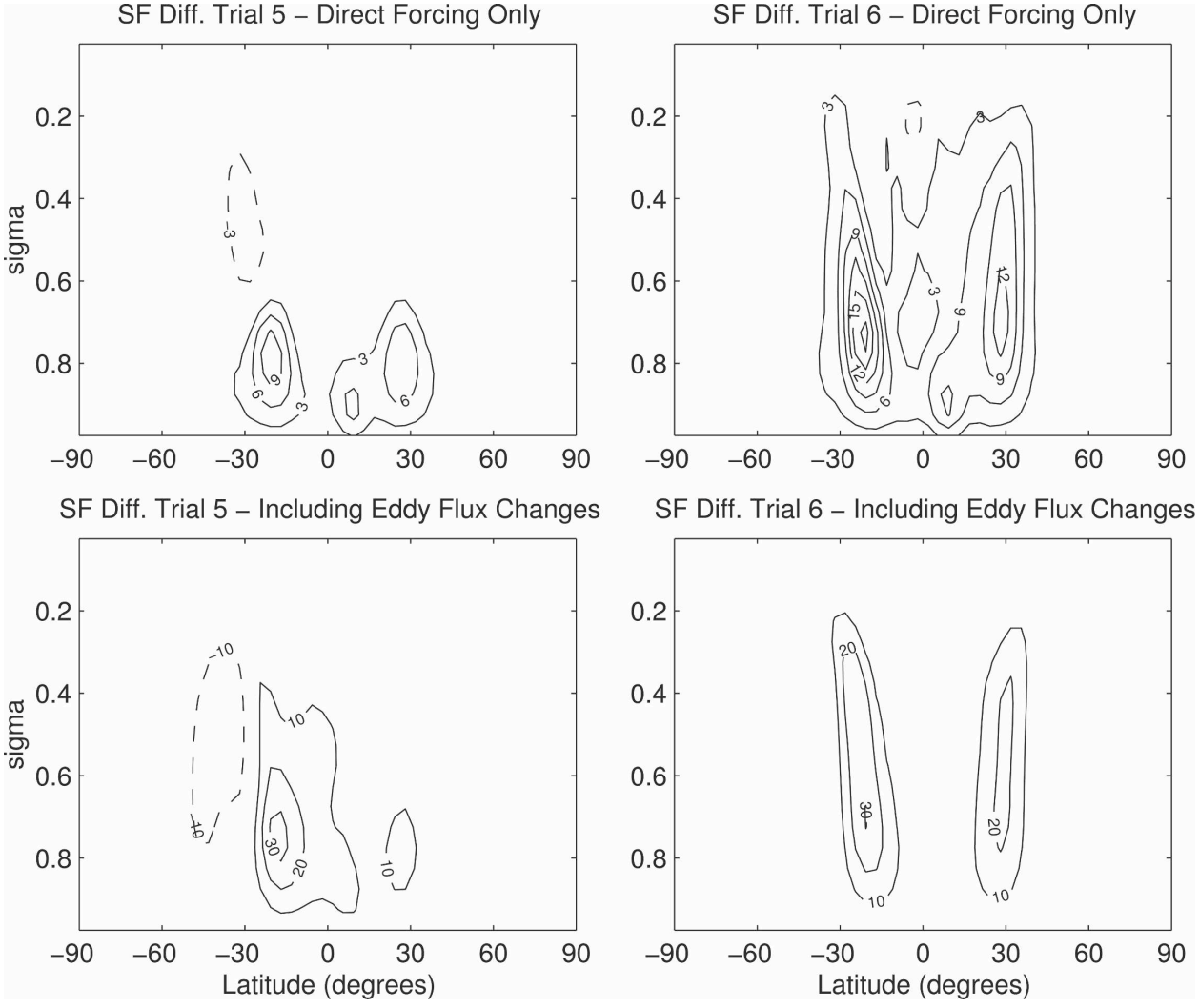

FIG. 18. As in Fig. 16, but for the streamfunction. Contour interval is 3×10^9 kg s^{-1} in top two panels and 10×10^9 kg s^{-1} in bottom two panels.

pospheric response (Kushner and Polvani 2004; Song and Robinson 2004), and the eddy–mean flow feedback that amplifies the response to forcing in this model may also enhance the response to a small perturbation descending from the stratosphere.

The results of this study show that the annular mode is the favored response of the atmosphere to a number of artificial forcings. As noted in the introduction, annular mode–like responses have been associated with greenhouse forcing and Antarctic ozone loss. The annular mode is featured in the discussion about stratosphere–troposphere coupling as well. If the annular modes are indeed a preferred forced response of the earth's atmosphere, then the attention they have received in recent years is well justified, and the annular modes should be considered when investigating problems in the extratropical dynamics of the earth's atmosphere.

Acknowledgments. This work was supported by the National Science Foundation through Grant ATM-0314094.

REFERENCES

Baldwin, M. P., and T. J. Dunkerton, 1999: Propagation of the Arctic Oscillation from the stratosphere to the troposphere. *J. Geophys. Res.,* **104,** 30 937–30 946.

——, and ——, 2001: Stratospheric harbingers of anomalous weather regimes. *Science,* **294,** 581–584.

Cash, B. A., P. J. Kushner, and G. K. Vallis, 2002: The structure and composition of the annular modes in an aquaplanet general circulation model. *J. Atmos. Sci.,* **59,** 3399–3414.

Edmon, H. J., Jr., B. J. Hoskins, and M. E. McIntyre, 1980: Elias-

sen–Palm cross-sections for the troposphere. *J. Atmos. Sci.,* **37,** 2600–2616.

Fyfe, J. C., G. J. Boer, and G. M. Flato, 1999: The Arctic and Antarctic Oscillations and their projected changes under global warming. *Geophys. Res. Lett.,* **26,** 1601–1604.

Gillett, N. P., M. R. Allen, R. E. McDonald, C. A. Senior, D. T. Shindell, and G. A. Schmidt, 2002: How linear is the Arctic Oscillation response to greenhouse gases? *J. Geophys. Res.,* **107,** 4022, doi:10.1029/2001JD000589.

Held, I. M., and M. J. Suarez, 1994: A proposal for the intercomparison of the dynamical cores of atmospheric general circulation models. *Bull. Amer. Meteor. Soc.,* **75,** 1825–1830.

Kidson, J. W., and I. G. Watterson, 1999: The structure and predictability of the "high-latitude mode" in the CSIRO9 general circulation model. *J. Atmos. Sci.,* **56,** 3859–3873.

Kushner, P. J., and L. M. Polvani, 2004: Stratosphere–troposphere coupling in a relatively simple AGCM: The role of eddies. *J. Climate,* **17,** 629–639.

——, I. M. Held, and T. L. Delworth, 2001: Southern Hemisphere atmospheric circulation response to global warming. *J. Climate,* **14,** 2238–2249.

Limpasuvan, V., and D. L. Hartmann, 2000: Wave-maintained annular modes of climate variability. *J. Climate,* **13,** 4414–4429.

Lorenz, D. J., and D. L. Hartmann, 2001: Eddy–zonal flow feedback in the Southern Hemisphere. *J. Atmos. Sci.,* **58,** 3312–3327.

——, and ——, 2003: Eddy–zonal flow feedback in the Northern Hemisphere winter. *J. Climate,* **16,** 1212–1227.

Polvani, L. M., and P. J. Kushner, 2002: Tropospheric response to stratospheric perturbations in a relatively simple general circulation model. *Geophys. Res. Lett.,* **29,** 1114, doi:10.1029/2001GL014284.

Rind, D., P. Lonergan, N. K. Balachandran, and D. Shindell, 2002: $2 \times CO_2$ and solar variability influences on the troposphere through wave-mean flow interactions. *J. Meteor. Soc. Japan,* **80,** 863–876.

Robinson, W. A., 1994: Eddy feedbacks on the zonal index and eddy–zonal flow interactions induced by zonal flow transience. *J. Atmos. Sci.,* **51,** 2553–2562.

——, 1996: Does eddy feedback sustain variability in the zonal index? *J. Atmos. Sci.,* **53,** 3556–3569.

——, and J. Qin, 1992: Predictability of the zonal index in a global model. *Tellus,* **44A,** 331–338.

Shindell, D. T., R. L. Miller, G. A. Schmidt, and L. Pandolfo, 1999: Simulation of recent northern winter climate trends by greenhouse-gas forcing. *Nature,* **399,** 452–455.

——, G. A. Schmidt, R. L. Miller, and D. Rind, 2001: Northern Hemisphere winter climate response to greenhouse gas, ozone, solar, and volcanic forcing. *J. Geophys. Res.,* **106,** 7193–7210.

Simmons, A. J., and D. M. Burridge, 1981: An energy and angular-momentum conserving vertical finite-difference scheme and hybrid vertical coordinates. *Mon. Wea. Rev.,* **109,** 758–766.

Song, Y., and W. A. Robinson, 2004: Dynamical mechanisms for stratospheric influences on the troposphere. *J. Atmos. Sci.,* **61,** 1711–1725.

Thompson, D. W. J., and J. M. Wallace, 1998: The Arctic Oscillation signature in the wintertime geopotential height and temperature fields. *Geophys. Res. Lett.,* **25,** 1297–1300.

——, and ——, 2000: Annular modes in the extratropical circulation. Part I: Month-to-month variability. *J. Climate,* **13,** 1000–1016.

——, and S. Solomon, 2002: Interpretation of recent Southern Hemisphere climate change. *Science,* **296,** 895–899.

——, J. M. Wallace, and G. C. Hegerl, 2000: Annular modes in the extratropical circulation. Part II: Trends. *J. Climate,* **13,** 1018–1036.

Vallis, G. K., E. P. Gerber, P. J. Kushner, and B. A. Cash, 2004: A mechanism and simple dynamical model of the North Atlantic Oscillation and annular modes. *J. Atmos. Sci.,* **61,** 264–280.

Yu, J.-Y., and D. L. Hartmann, 1993: Zonal flow vacillation and eddy forcing in a simple GCM of the atmosphere. *J. Atmos. Sci.,* **50,** 3244–3259.